Lifetime-Oriented Droop Control Strategy for AC Islanded Microgrids

Wang, Yanbo; Liu, Dong; Liu, Ping; Deng, Fujin; Zhou, Dao; Chen, Zhe

Published in:
I E E E Transactions on Industry Applications

DOI (link to publication from Publisher):
10.1109/TIA.2019.2898847

Publication date:
2019

Document Version
Accepted author manuscript, peer reviewed version

This article has been accepted for publication in a future issue of this journal, but has not been fully edited. Content may change prior to final publication. Citation information: DOI 10.1109/TIA.2019.2898847, IEEE Transactions on Industry Applications

Lifetime-Oriented Droop Control Strategy for AC Islanded Microgrids

Yanbo Wang, *Member, IEEE*, Dong Liu, *Member, IEEE,* Ping Liu, *Member, IEEE*, Fujin Deng, *Member, IEEE,* Dao Zhou, *Senior Member, IEEE,* Zhe Chen, *Fellow, IEEE*

***Abstract*— This paper presents a lifetime-oriented droop control strategy for AC islanded microgrids, which is able to perform equal thermal sharing among paralleled inverters. Electro-thermal model and temperature estimation model are first established to estimate thermal characteristics of inverters, and temperature-power droop relationships are built according to the electro-thermal model. Then, a lifetime-oriented droop controller is developed to realize equal thermal stress sharing. In addition, small signal model of microgrid equipped with the proposed droop control is established, and the effect of electro-thermal parameters of power devices on closed-loop stability of droop controller is investigated. Simulation and experimental results show that the proposed lifetime-oriented droop control is able to perform identical thermal stress sharing among paralleled inverters automatically, which mitigates the impact of thermal stresses on average lifetime of inverters, and thus enhances long-term reliability of microgrids.**

Keywords*— Droop control, lifetime, paralleled inverters, thermal sharing, AC islanded microgrid.

I. INTRODUCTION

Ongoing research efforts in past decades have been implemented to promote application of small-scale autonomous power systems such as microgrids and active distribution networks [1]-[2]. As one of important components in future power system, microgrids are able to enhance flexibilities and reliability of electricity supply. Microgrids can be operated either in grid-connected mode or autonomous islanded mode according to power system demands.

In autonomous islanding mode, power regulations are dictated by micro sources themselves. Droop control strategies have been widely proposed to perform proportional power sharing among paralleled inverters [1]-[3]. The attractive advantage of droop control is to automatically assign output power among inverters without using critical communication facilities, which thus improves reliability and flexibility of distributed power systems. Existing droop control strategies commonly perform proportional power sharing according to maximum ratings of DG inverters [1]-[4]. To improve the accuracy of power sharing, various droop control strategies with adaptive virtual impedance [4], state estimation [2] and disturbance injection [3] have been proposed. In addition, several novel droop control strategies with consideration of cost optimization [5], intermittent effect mitigation of renewable energies [6] have been presented to improve stead-state performance of power sharing in islanded microgrids. In fact, the microgirds tend to be used to supply reliable electricity for critical loads in safe-critical systems, such as ship microgrid, aircraft power system, and remote microgrid [7]-[8]. Hence, reliability and safety are becoming essential concerns in microgrids dominated by critical loads. The efforts toward reliability enhancement should be further explored. However, these research aspects have not ever been addressed in droop-controlled microgrids.

It is well-known that operating temperatures of power devices have significant impacts on long-term reliability of power electronic system, where over-temperature and temperature fluctuations caused by power semiconductors losses are the critical factors of power devices failures [9]. Fig. 1 shows the typical junction temperature profile of power device. Once power devices are continuously operated at a junction temperature above the maximum temperature (T_{j_max}), the failure of power devices may happen [9].

In practical operation of microgrids, thermal operating points of inverters may be different due to differences of power semiconductor and aging impact [10]-[12]. The unequal thermal stress distribution among paralleled inverters may be caused by the difference of inverter parameters, which thus mitigates long-term reliability of microgrids. Thermal management is becoming an important aspect of power electronic systems with the increasing demands of high reliability [13]. Active thermal control strategies by reducing or redistributing load power have been introduced to improve system efficiency and increase the average lifetime of inverters [13]. To improve long-term reliability of power converters, an active thermal control-based current sharing scheme for paralleled inverters is proposed in [10], where the effect of parameters variation on temperature is investigated and load current is redistributed among paralleled inverters according to their temperature difference. A dynamic electro-thermal model is established to estimate transient junction temperature of semiconductor devices in [13], and then power sharing among paralleled inverters is facilitated according to estimated junction temperature. The proposed method is able to improve overall system

This article has been accepted for publication in a future issue of this journal, but has not been fully edited. Content may change prior to final publication. Citation information: DOI 10.1109/TIA.2019.2898847, IEEE Transactions on Industry Applications

efficiency and reliability. However, the communication link is required to support the proposed control method.

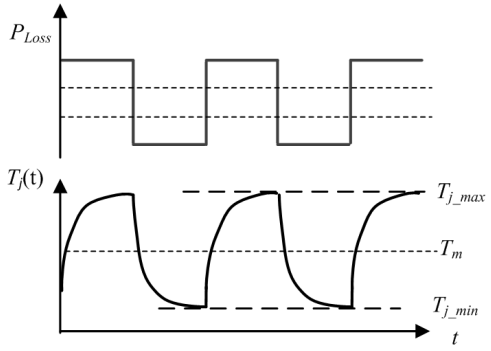

Fig. 1. Junction temperature profile of semiconductor device [9]

Existing droop control strategies merely focus on active thermal management in microgrids. To enhance long-term system reliability, a lifetime-oriented droop control strategy is developed in this paper as an extension of our previous work [14]. The thermal issues are related with power semiconductor and filter, but power semiconductors have more significant effects on thermal issue than other factors. Hence, the equal thermal issue caused by difference of power semiconductors is mainly concerned in this work. An electro-thermal model is first built, and temperature estimation model is established to observe thermal distribution among paralleled inverters. Then, the lifetime-oriented droop control strategy is proposed to perform active thermal sharing. The proposed method is able to redistribute thermal dissipation and mitigate the thermal stresses, which also preserves the inherent advantage of conventional droop control. The main contributions of this paper are: (1) A lifetime-oriented droop control scheme with active thermal balance is developed. (2) Virtual impedance is developed in the proposed droop control strategy to enhance sharing accuracy of thermal stress. (3) Small signal model of microgrid equipped with the proposed droop controller is established, and the effect of electro-thermal parameters on controller stability is investigated.

The rest of this paper is organized as follows. In Section II, the conventional droop control scheme is reviewed. In Section III, electro-thermal model and temperature estimation model is established to observe the thermal behavior of inverters. The lifetime-oriented droop control strategy is presented in Section IV. In Section IV and V, simulation and experimental results are given to validate the lifetime-oriented droop control. The conclusions are drawn in Section VI.

II. Conventional Droop Control Strategy

Droop control strategies have been widely proposed to perform proportional power sharing in islanded microgrids. Fig. 2 shows the circuit configuration of a droop-controlled microgrid, where active power-frequency (P-ω) and reactive power-voltage (Q-V) droop control strategy is employed to perform power sharing. The basic principle of droop control strategy is illustrated in Fig. 3. The mathematical relationship of droop controller is represented as (1) and (2) [2]

$$\omega_i^* = \omega_0 - m_i P_i \tag{1}$$

$$V_{oi}^* = V_0 - n_i Q_i \tag{2}$$

ω^*_i and V^*_{oi} are output angle frequency and voltage of i-th inverter. P_i and Q_i are output active power and reactive power of i-th inverter. m_i and n_i are droop coefficients. ω_0 and V_0 are initial angle frequency and voltage at no load.

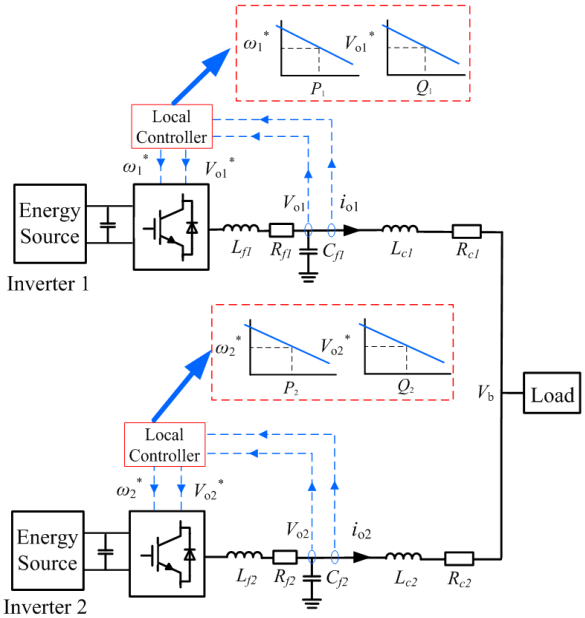

Fig. 2 The circuit configuration of droop-controlled microgrids

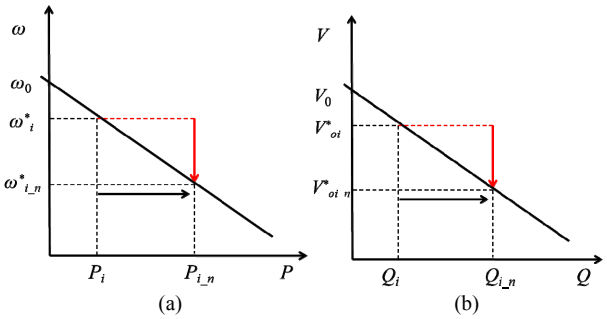

Fig. 3 The diagram of droop control strategy

The initial operating points of power controller are (P_i, ω^*_i) and (Q_i, V^*_{oi}). In the presence of load disturbances, the terminal frequency and voltage of DG inverter will be changed to track output power. Then, power controller is transferred into new operating point (P_{i_n}, $\omega^*_{i\_n}$) and (Q_{i_n}, $V^*_{oi\_n}$). The droop coefficients tend to be tuned according to respective maximum ratings of DG units as (3) and (4) [1]-[4].

$$m_1 P_{\max 1} = m_2 P_{\max 2} = \ldots = m_i P_{\max i} = \omega_{\min} - \omega_{\max} \tag{3}$$

$$n_1 Q_{\max 1} = n_2 Q_{\max 2} = \ldots = n_i Q_{\max i} = V_{\min} - V_{\max} \tag{4}$$

where $P_{\max i}$ and $Q_{\max i}$ are maximum active power and reactive power capacity of i-th inverter.

However, the difference of power devices, even if in inverters with equal ratings, can cause different thermal operating points. Therefore, the unequal thermal stress may occur due to the difference of these parameters, which weakens long-term reliability of microgrids. Thus,

This article has been accepted for publication in a future issue of this journal, but has not been fully edited. Content may change prior to final publication. Citation information: DOI 10.1109/TIA.2019.2898847, IEEE Transactions on Industry Applications

this paper presents a lifetime-oriented droop control method to perform equal thermal sharing among paralleled inverters.

III. Proposed Lifetime-Oriented Droop Control Strategy

In this section, a lifetime-oriented droop control strategy is proposed. Electro-thermal model is first established to estimate the temperature-current characteristic. Then, the temperature-current characteristic is incorporated into droop controller. Afterwards, power sharing can be performed by the lifetime-oriented droop control strategy. The aim of electro-thermal modeling is to compute the average junction temperatures of power devices and establish temperature-power relationship, which is taken into account by droop controller.

A. Electro-thermal modeling

Power loss in a voltage-source converter is composed of conduction loss and switching loss of power devices [13]. The average conduction losses of IGBT (P_{con_IGBT}) and diode (P_{con_Diode}) during the fundamental period may be represented as (5) and (6) [15].

$$P_{con\_IGBT} = \frac{1}{T_0}\int_0^{T_0/2}(V_{ce0} + rI_m\sin(\omega t))*I_m\sin(\omega t)*(\frac{1}{2}(1+m\sin(\omega t+\varphi)))dt$$
$$= \frac{1}{2}(V_{ce0}\frac{I_m}{\pi} + r\frac{I_m^{\,2}}{4}) + m\cos\varphi(V_{ce0}\frac{I_m}{8} + \frac{1}{3\pi}rI_m^{\,2}) \tag{5}$$

$$P_{con\_Diode} = \frac{1}{T_0}\int_0^{T_0/2}(V_{ce0} + rI_m\sin(\omega t))*I_m\sin(\omega t)*(\frac{1}{2}(1-m\sin(\omega t+\phi)))dt$$
$$= \frac{1}{2}(V_{T0}\frac{I_m}{\pi} + r\frac{I_m^{\,2}}{4}) - m\cos\phi\cdot(V_{T0}\frac{I_m}{8} + \frac{1}{3\pi}rI_m^{\,2}) \tag{6}$$

where T_0 is fundamental period, V_{ce0} is the constant voltage drop and r is the current magnitude dependent voltage in output characteristic of on-state voltage and collector current from datasheet [15]. I_m is amplitude of load current. m is modulation index related to the AC voltage amplitude and DC-link voltage. φ is the phase angle between voltage and current. ω is fundamental angle frequency. The average switching losses of IGBT [15] over a fundamental period can be given as (7).

$$P_{sw\_IGBT} = \frac{1}{T_0}\sum_1^n E_{sw}(i) \tag{7}$$

E_{sw} is the sum of turn-on and turn-off energy dissipation, which is given as (8).

$$E_{sw}(i) = (E_{on}(I_{nom},V_{nom}) + E_{off}(I_{nom},V_{nom}))\frac{i}{I_{nom}}\cdot\frac{V_{dc}}{V_{nom}} \tag{8}$$

The reverse recovery loss of diode can be calculated [15] as (9).

$$P_{rec\_diode} = \frac{1}{\pi}f_{sw}*E_{rec}(I_{nom})*(0.45\frac{i}{I_{nom}} + 0.55)*\frac{V_{dc}}{V_{nom}} \tag{9}$$

E_{on} and E_{off} are measured turn-on and turn-off energy dissipation of IGBT from datasheet. i is phase leg current. I_{nom} and V_{nom} are nominal current and voltage of power device. V_{dc} is DC-link voltage in practical application, which may be different from the nominal DC voltage. E_{rec} is reverse recovery loss of diode.

Then, the total power loss of IGBTs and diodes can be represented as (10)-(11) by combining (5)-(9).

$$P_{loss\_IGBT} = P_{con\_IGBT} + P_{sw\_IGBT} \tag{10}$$

$$P_{loss\_Diode} = P_{con\_Diode} + P_{rec\_Diode} \tag{11}$$

B. Temperature estimation model

To investigate influence of load current on temperature, the temperature estimation model is established. Junction temperature of power devices in DG inverters can be estimated by RC equivalent thermal models [16]-[17], which provide effective solutions to estimate junction temperature without direct measurements.

Thermal resistance is a critical parameter to determine thermal behavior of power electronic devices. In practical operation of inverters, the thermal distribution would be different due to the difference of thermal resistance. Fig.4 shows the thermal resistance chain of individual power devices applied in this paper [16], where each current source represents the power losses of power device. $R_{\text{thJC\_IGBT}}$ and $R_{\text{thJC\_D}}$ are thermal resistance of IGBT and diode from junction to case. $R_{\text{thCH\_IGBT}}$ and $R_{\text{thCH\_D}}$ are thermal resistance of IGBT and diode from case to heat sink. R_{thHA} is thermal resistance from heat sink to ambient temperature.

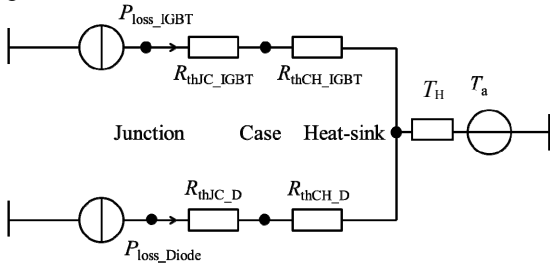

Fig. 4. Equivalent thermal model of semiconductor power device [15].

Then, the junction temperature of IGBT and diode can be derived from the equivalent thermal model [16] as shown in Fig. 4 as (12) and (13).

$$T_{jun\_T} = P_{loss\_IGBT}\cdot(R_{thJC\_IGBT} + R_{thCH\_IGBT}) + T_H \tag{12}$$

$$T_{jun\_D} = P_{loss\_Diode}\cdot(R_{thJC\_D} + R_{thCH\_D}) + T_H \tag{13}$$

where T_{jun_T} and T_{jun_D} are junction temperature of IGBT and diode, T_H is heat-sink temperature.

C. Implementation of lifetime-oriented droop control

With the assumption that three-phase load is balanced, IGBTs and diodes of each inverter have same thermal characteristics. Thus, the temperature of power devices is used as temperature indicator of inverter. The temperature-current relationship of inverters can be derived from (12) and (13). In this paper, a microgrid with two inverters is used to exemplify the proposed droop control strategy, where different IGBT power devices are applied in different inverters. The types and parameters of power devices applied to calculate electro-thermal characteristics are given in Table I [18]-[19].

As shown in Fig.5, the temperature-current relationship of different inverters can be obtained by using (12)-(13) and parameters in Table I. It can be observed that inverters have different thermal-electro parameters due to the difference of semiconductor power devices.

This article has been accepted for publication in a future issue of this journal, but has not been fully edited. Content may change prior to final publication. Citation information: DOI 10.1109/TIA.2019.2898847, IEEE Transactions on Industry Applications

Furthermore, the mathematical representation of temperature-current relationship is obtained from Fig.5 by using least square fitting, which is given as (14)-(15).

$$T_{IGBT}(I_c) = a_1 I_c^{\ 2} + b_1 I_c + c_1 \tag{14}$$

$$T_{Diode}(I_c) = a_2 I_c^{\ 2} + b_2 I_c + c_2 \tag{15}$$

TABLE I
PARAMETERS APPLIED IN ELECTRO-THERMAL MODEL

Inverter1		Inverter2	
Power Rating	2kW	Power Rating	2kW
Power Device	FP10R06KL4	Power Device	FS6R06VE3_B2
R_{thJC_IGBT}	2.2 K/W	R_{thJC_IGBT}	3.3 K/W
R_{thCH_IGBT}	0.29 K/W	R_{thCH_IGBT}	1.3 K/W
R_{thJC_D}	3.5 K/W	R_{thJC_D}	4.5 K/W
R_{thCH_D}	1.1 K/W	R_{thCH_D}	2.1 K/W
Current (Based value)	12 A	Temperature (Based value)	75°C
Frequency (Based value)	50Hz	Voltage (Based value)	110V
a_1(Inverter1)	0.0523	a_1(Inverter2)	0.1344
b_1(Inverter1)	1.7771	b_1(Inverter2)	2.5495
c_1(Inverter1)	24.943	c_1(Inverter2)	25.06

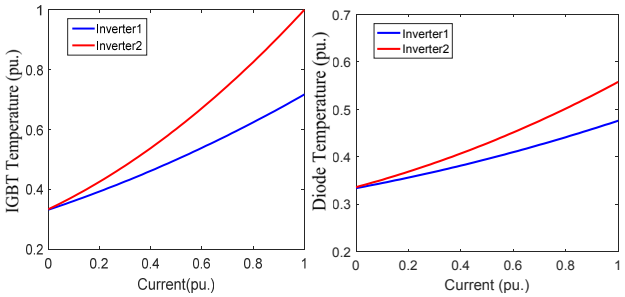

(a) (b)

Fig. 5. Temperature-current relationship of inverter 1 and inverter 2. (a) Output current-dependent IGBT junction temperature. (b) Output current-dependent diode junction temperature.

where $T_{IGBT}(I_c)$ and $T_{Diode}(I_c)$ are loading current-dependent junction temperature of IGBT and diode. $a_1, b_1, c_1, a_2, b_2, c_2$ are coefficients of fitted equations, which reveals characteristics of electro-thermal parameters. The coefficients are obtained according to Fig. 5. For power devices applied in this paper, these parameters are given in Table I.

Once temperature-current characteristic (14)-(15) is obtained, it can be incorporated into droop curves to perform thermal sharing control. Then, new active power-frequency and reactive power-voltage droop relationships with consideration of active thermal balance are established as (16)-(20).

$$\omega_i^* = \omega_{\max} - \Delta\omega_i \tag{16}$$

$$\Delta\omega_i = \frac{\omega_{\max} - \omega_{\min}}{P_{\max}(T_{IGBT\_max})} \times T_{IGBT}\left(\frac{P_i}{V_{nom}}\right) \tag{17}$$

$$V_{oi}^* = V_{\max} - \Delta V_{oi} \tag{18}$$

$$\Delta V_{oi} = \frac{V_{\max} - V_{\min}}{Q_{\max}(T_{IGBT\_max})} \times T_{IGBT}\left(\frac{Q_i}{V_{nom}}\right) \tag{19}$$

$$\text{or } \Delta V_{oi} = \frac{V_{\max} - V_{\min}}{Q_{\max}(T_{Diode\_max})} \times T_{Diode}\left(\frac{Q_i}{V_{nom}}\right) \tag{20}$$

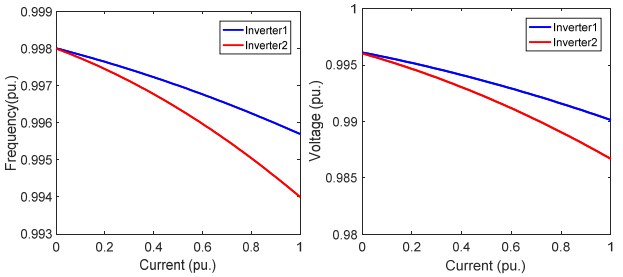

(a) (b)

Fig. 6. The proposed lifetime-oriented droop control. (a) The temperature-dependent *P-f* droop curve. (b) The temperature-dependent *Q-V* droop curve.

It can be seen that the proposed droop controller (16) and (18) are nonlinear equations associated with temperature characteristics. The proposed *P-f* droop curves and *Q-V* droop curves are shown in Fig. 6. Compared with the conventional linear droop control strategies, the proposed droop control scheme is able to perform thermal sharing according to temperature difference of inverters. The inverter with lower temperature will generate more powers. Then, the thermal stress would be redistributed, which thus achieves equal thermal distributions among paralleled inverters. The temperature-dependent droop characteristic can be defined according to thermal models of different power devices.

Fig. 7 shows the diagram of the proposed droop control scheme. Power loss and thermal characteristic are calculated according to offline electro-thermal model established in section III. Then, the temperature-dependent droop controller is formulated by incorporating thermal characteristics.

For reactive power-voltage droop controller, either IGBT or diode junction temperature may be selected as control objective. It is well-known that the accuracy of reactive power sharing is commonly affected by unbalanced feeder impedances [3], [20]. To eliminate the reactive sharing errors, inverter equivalent fundamental impedance can be reshaped by virtual impedance methods. For the lifetime-oriented droop controller, the accuracy of thermal sharing may be affected if only reactive power loads are fed. To guarantee the accuracy of thermal sharing, the following constraint (21) on inverter equivalent fundamental impedances is performed, where virtual impedance is configured into droop controller to reshape the terminal output performance as (22).

$$X_{f1} \cdot Q_{\max 1}(T_{jun1}) = X_{f2} \cdot Q_{\max 2}(T_{jun2}) \tag{21}$$

$$\frac{Q_{\max 1}(T_{jun1})}{Q_{\max 2}(T_{jun2})} = \frac{X_{f2}}{X_{f1}} = \frac{X_{o2} + X_{v2}}{X_{o1} + X_{v1}} \tag{22}$$

$Q_{maxi}(T_{juni})$ is junction temperature-dependent reactive power capacity of *i*-th inverter. X_{fi} is the desired inverter equivalent fundamental impedance. X_{oi} is the closed-loop output impedance of *i*-th inverter at fundamental frequency. X_{vi} is virtual fundamental impedance of *i*-th

This article has been accepted for publication in a future issue of this journal, but has not been fully edited. Content may change prior to final publication. Citation information: DOI 10.1109/TIA.2019.2898847, IEEE Transactions on Industry Applications

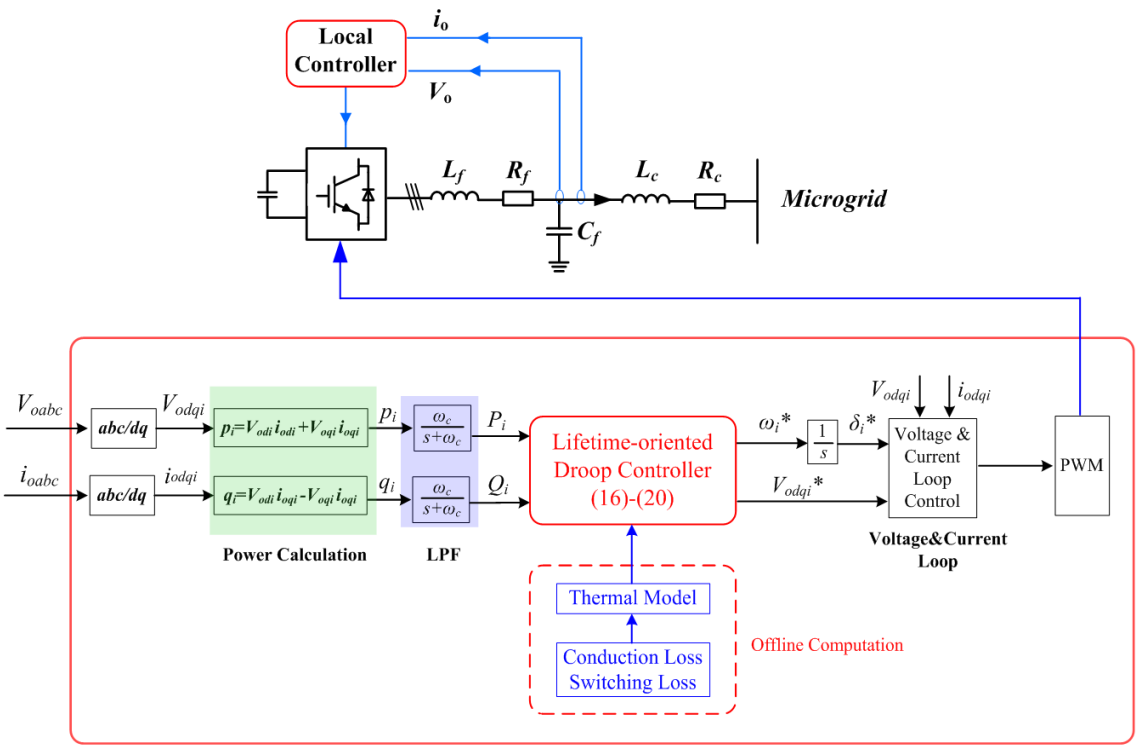

Fig.7. The diagram of proposed lifetime-oriented droop control strategy

inverter. Then, the reference voltage incorporating virtual impedance can be derived as (23) and (24). The control diagram is shown in Fig. 8.

$$V_{refi\_d}=V_{odi}^{*}-(R_{vi}\cdot I_{odi}-\omega_0 L_{vi}I_{oqi}) \tag{23}$$

$$V_{refi\_q}=V_{oqi}^{*}-(R_{vi}\cdot I_{oqi}+\omega_0 L_{vi}I_{odi}) \tag{24}$$

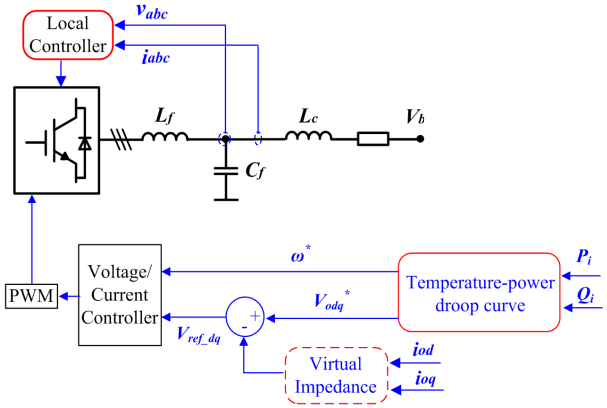

Fig. 8. The control diagram of proposed droop controller with virtual impedance.

D. Small signal modelling and stability analysis

Stability of droop controller is an important aspect for islanded microgrids. Previous small signal model of microgrids including droop controller, voltage control, current controller as well as active loads have been widely established in [21]-[26], where the effects of droop controller and active loads on small signal stability are investigated. In this section, small signal model of microgrid equipped with lifetime-oriented droop controller is built. And small signal stability is investigated, where the effect of electro-thermal parameters of power devices on stability is revealed.

Dynamic equation of angle relationship of the *i*-th inverter on *dq*-frame is represented as shown in Fig.7 as (25).

$$\dot{\delta}_i=\omega_i-\omega_{com} \tag{25}$$

where δ_i and ω_i are phase angle and angle frequency of inverter (i=1,2). ω_{com} is rotating frequency of common reference frame. As shown in Fig.7, the average active power (P_i) and reactive power (Q_i) of *i*-th inverter can be represented by instantaneous active power (p_i) and reactive power (q_i) passing low pass filter as (26) and (27).

$$P_i=\frac{\omega_c}{s+\omega_c}(V_{odi}i_{odi}+V_{oqi}i_{oqi}) \tag{26}$$

$$Q_i=\frac{\omega_c}{s+\omega_c}(V_{odi}i_{oqi}-V_{oqi}i_{odi}) \tag{27}$$

Small signal equations of the proposed droop controller can be derived by combining and linearizing (16)-(19) as (28)-(31).

$$\Delta\omega_i^{*}=-\frac{\omega_{\max}-\omega_{\min}}{P_{\max}(T_{IGBT\_\max})}\Delta T_{IGBT\_i} \tag{28}$$

$$\Delta T_{IGBT\_i}=\frac{(2a_1P_{i0}+b_1)}{V_{nom}}\Delta P_i \tag{29}$$

$$\Delta V_{odi}^{*}=-\frac{V_{\max}-V_{\min}}{Q_{\max}(T_{IGBT\_\max})}\Delta T_{Diode\_i},\ \Delta V_{oqi}^{*}=0 \tag{30}$$

$$\Delta T_{Diode\_i}=\frac{(2a_1Q_{i0}+b_1)}{V_{nom}}\Delta Q_i \tag{31}$$

The new active power-frequency and reactive power-voltage droop coefficients can be defined by combining (28)-(29) and (30)-(31) as (32) and (33). It can be seen that the new droop coefficients are associated with

This article has been accepted for publication in a future issue of this journal, but has not been fully edited. Content may change prior to final publication. Citation information: DOI 10.1109/TIA.2019.2898847, IEEE Transactions on Industry Applications

electro-thermal parameters of power devices, which have effects on closed-loop stability of droop controller.

$$m_i = -\frac{\omega_{\max}-\omega_{\min}}{P_{\max}(T_{IGBT\_\max})}\cdot\frac{(2a_1P_{i0}+b_1)}{V_{nom}} \quad (32)$$

$$n_i = -\frac{V_{\max}-V_{\min}}{Q_{\max}(T_{IGBT\_\max})}\cdot\frac{(2a_1Q_{i0}+b_1)}{V_{nom}} \quad (33)$$

Then, small signal dynamic equations of IGBT average junction temperature and diode average junction temperature are derived by linearizing (26)-(27) and combining (26) and (29) as (34) and (35).

$$\Delta\dot{T}_{IGBT} = \frac{(2a_1P_{i0}+b_1)}{V_{nom}}\omega_c(-\Delta P_i + V_{odi0}\Delta i_{odi} + i_{odi0}V_{odi}) \quad (34)$$

$$\Delta\dot{T}_{Diode} = \frac{(2a_1Q_{i0}+b_1)}{V_{nom}}\omega_c(-\Delta Q_i + V_{odi0}\Delta i_{oqi} + i_{oqi0}\Delta V_{odi}) \quad (35)$$

The average junction temperature of IGBT and Diode are incorporated in small signal model as state variables.

The small signal dynamic equation of output current of *i*-th DG inverter in *dq*-frame is given as (36).

$$\begin{aligned}\dot{i}_{odi} &= -\frac{R_{ci}}{L_{ci}}i_{odi} - \omega_i i_{oqi} + \frac{1}{L_{ci}}V_{odi} - \frac{1}{L_{ci}}V_{bd} \quad (i=1,2)\\ \dot{i}_{oqi} &= -\frac{R_{ci}}{L_{ci}}i_{oqi} + \omega_i i_{odi} + \frac{1}{L_{ci}}V_{oqi} - \frac{1}{L_{ci}}V_{bq} \quad (i=1,2)\end{aligned} \quad (36)$$

Then, small signal model of individual inverter considering junction temperature dynamic of power device is formulated by combining and linearizing (25)-(36) as (37).

$$\Delta\dot{x}_{invi} = A_{invi}\Delta x_{invi} + B_{invi}\Delta V_{bdq} \quad (i=1,2) \quad (37)$$

where $\Delta x_{invi} = \left[\Delta\delta_i, \Delta P_i, \Delta Q_i, \Delta V^*_{odqi}, \Delta i_{odqi}, \Delta T_{IGBT}, \Delta T_{Diode}\right]^T$, A_{invi} and B_{invi} are parameters matrices, which are given in Appendix. Similarly, small signal model of inverter2 can be established by aforementioned procedure in the form of state-space form. In this work, the local reference dq frame of inverter1 is defined as common DQ reference frame. And inverter2 is transferred to the common frame by using transformation equation [2], [21].

Dynamic equations of RL load is established as (38).

$$\begin{aligned}\dot{i}_{LoadD} &= -\frac{R_{Load}}{L_{Load}}i_{LoadD} - \omega_1 i_{LoadD} + \frac{1}{L_{Load}}V_{bD}\\ \dot{i}_{LoadQ} &= -\frac{R_{Load}}{L_{Load}}i_{LoadQ} + \omega_1 i_{LoadQ} + \frac{1}{L_{Load}}V_{bQ}\end{aligned} \quad (38)$$

Then, small signal dynamic equation of RL load is established on DQ reference frame by linearizing (38) as (39).

$$\Delta\dot{i}_{LoadDQ} = A_{Load1}\Delta\omega_1 + A_{Load2}\Delta i_{LoadDQ} + A_{Load3}V_{bDQ} \quad (39)$$

To establish voltage equation, virtual resistors are introduced between node and ground to define bus voltage [21]. The bus voltage (V_b) can be represented on common DQ frame as (40).

$$V_{bDQ} = R_N(i_{o1DQ} + i_{o2DQ} - i_{LoadDQ}) = R_N\cdot(T_1\cdot x_{inv1} + T_2\cdot x_{inv2} + i_{loadDQ}) \quad (40)$$

A_{Load1}, A_{Load2}, A_{Load3}, R_N, T_1 and T_2 are system parameter matrices, which are given in Appendix.

The complete small signal model of microgid as shown in Fig. 2 can be established as (41) by combining (37)-(40).

$$\Delta\dot{x}_{MG} = A_{MG}\Delta x_{MG} \quad (41)$$

$\Delta x_{MG} = \left[\Delta x_{inv1}, \Delta x_{inv2}, \Delta i_{loadDQ}\right]^T$, A_{MG} is system parameter matrix, which is given in Appendix. And initial conditions applied in small signal analysis are given in Table III in Appendix.

Fig. 9 shows the eigenvalues trajectory of state matrix (A_{MG}) as a function of active power-frequency droop coefficient (32). It can be seen that the eigenvalue trajectory will move toward right-half plane (unstable region) with increase of thermal impedance from 0.2 to 0.6. Fig. 10 demonstrates the eigenvalues trace of system state matrix (A_{MG}) as a function of reactive power-voltage droop coefficient (33), where eigenvalue trace moves toward unstable region as increase of thermal impedance from 0.2 to 0.6. The analysis results show that small signal stability of the proposed droop controller can be affected by electro-thermal parameters of power devices.

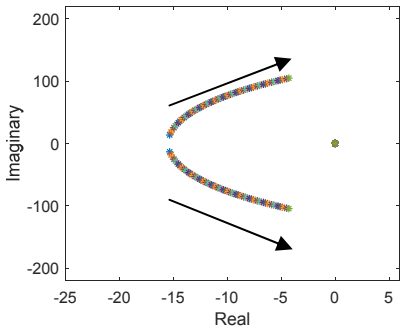

Fig. 9. Eigenvalue trajectory of low-frequency modes as a function of active power-frequency droop coefficient (32) with increase of thermal impedance from to 0.2 to 0.6.

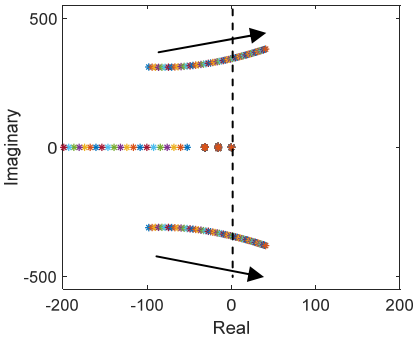

Fig. 10. Eigenvalue trajectory of low-frequency modes as a function of reactive power-voltage droop coefficient (33) with increase of thermal impedance from to 0.2 to 0.6.

IV. Simulation Verification

In order to validate the effectiveness of the lifetime-oriented droop control strategy, simulation verifications in MALAB with PLECS blockset are performed. The system parameters applied in simulation and experimental verification are given in Table II.

This article has been accepted for publication in a future issue of this journal, but has not been fully edited. Content may change prior to final publication. Citation information: DOI 10.1109/TIA.2019.2898847, IEEE Transactions on Industry Applications

TABLE II
SYSTEM PARAMETERS APPLIED IN SIMULATION AND EXPERIMENT

Parameters	Value	Parameters	Value
Switching frequency	10kHz	Frequency	50 Hz
DC voltage	400V	Base Voltage (Phase RMS)	150V
L_{f1}/R_{f1}	3mH/0.1Ω	L_{f2}/R_{f2}	3mH/0.1Ω
L_{c1}/R_{c1}	4mH/0.2Ω	L_{c2}/R_{c2}	4mH/0.2Ω
L_{Load}/R_{Load}	20mH/20Ω	C_{f1}/C_{f2}	25μF/25μF
ω_c	20π rad/s		

Fig. 11 shows simulation results of paralleled inverters with same power devices under conventional droop control method, where the Fig. 11(a) shows output active power of inverters and Fig. 11(b) shows IGBT average junction temperature of inverters when active power loads are increased. It can be seen that the proportional power sharing and equal thermal dissipation are performed.

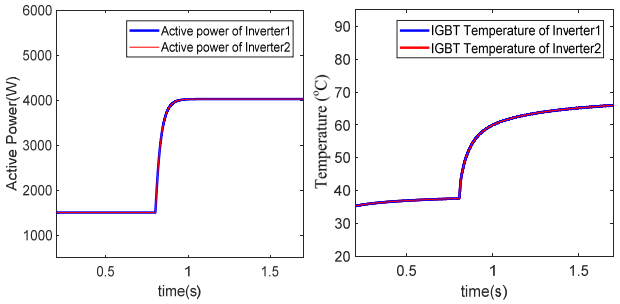

(a) (b)

Fig. 11. Simulated results of paralleled inverters with same power devices. (a) Active power sharing of inverters. (b) IGBT average junction temperature of inverters.

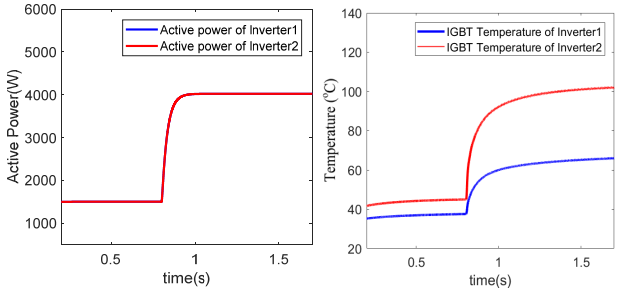

(a) (b)

Fig. 12. Simulated results of paralleled inverters with different power devices. (a) Active power sharing of inverters. (b) IGBT Average junction temperature of inverters.

Fig. 12 shows simulation results of paralleled inverters with different power devices under conventional droop control method. Although the proportional power sharing can be achieved, the thermal stresses are unequally distributed once different thermal impedance characteristics of inverters happens, which causes unbalanced thermal dissipation as shown in Fig. 12(b).

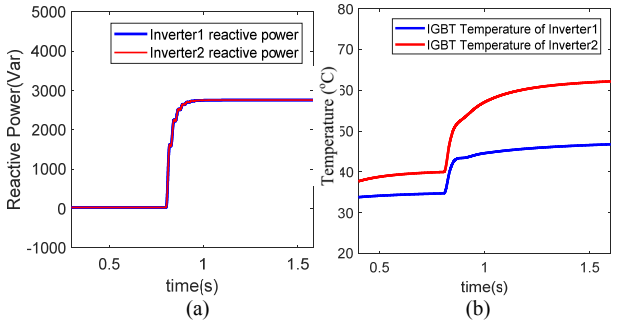

(a) (b)

Fig. 13. Simulated results of paralleled inverters with reactive power loads. (a) Reactive power sharing of inverters. (b) IGBT Average junction temperature of inverters.

Fig. 13 shows simulation results of paralleled inverters with reactive power loads. Although the reactive power can be equally shared, the thermal stresses are unequally distributed due to difference of thermal impedance characteristics as shown in Fig. 13(b). Hence, the conventional droop control method fails to deal with unequal thermal stress issue in microgrid.

Fig. 14 shows simulation results of paralleled inverters under proposed lifetime-oriented droop controller. Active power and IGBT average junction temperature of inverters are shown in Fig.14(a) and Fig.14(b). It can be observed that both proportional power sharing and equal thermal dissipation are performed. Compared with conventional droop control approach, the proposed lifetime-oriented droop control strategy can still perform same results if power devices of inverters are same, which thus preserves advantage of conventional droop control strategies.

Fig. 15 shows the simulation results of paralleled inverters with different power devices under the proposed lifetime-oriented droop controller. It can be seen from Fig. 15(b) that the proposed droop control strategy is able to share thermal stress automatically by regulating active powers of inverters, so that the thermal stress can be equally distributed between inverters.

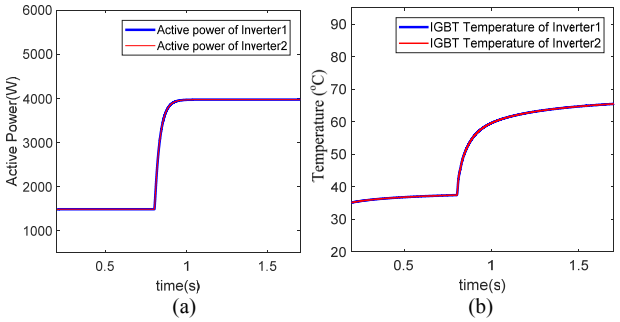

(a) (b)

Fig. 14 Simulated results of paralleled inverters with same power devices under the proposed lifetime-oriented droop controller. (a) Active power sharing of inverters. (b) IGBT average junction temperature of inverters.

This article has been accepted for publication in a future issue of this journal, but has not been fully edited. Content may change prior to final publication. Citation information: DOI 10.1109/TIA.2019.2898847, IEEE Transactions on Industry Applications

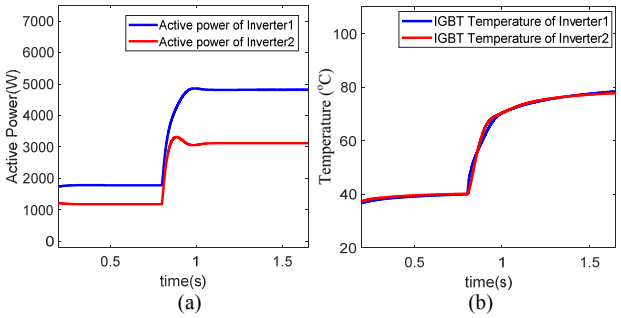

(a) (b)

Fig. 15 Simulated results of paralleled inverters with different power devices under the proposed lifetime-oriented droop controller. (a) Active power sharing of inverters. (b) IGBT average junction temperature of inverters.

Fig.16 shows the simulation results of paralleled inverters in the presence of reactive power increase, where virtual impedance loop is incorporated into the proposed droop controller. It can be seen from Fig. 16(b) that the droop controller is able to equally redistribute thermal stress between paralleled inverters by regulating reactive powers of inverters.

Fig.17 shows the simulated output power of paralleled inverters when active power and reactive power droop coefficients are increased due to electro-thermal parameters are perturbed. The simulation results show that the droop controller may become unstable if electro-thermal parameters are increased, which agrees with the theoretical analysis results shown in Fig. 9-10.

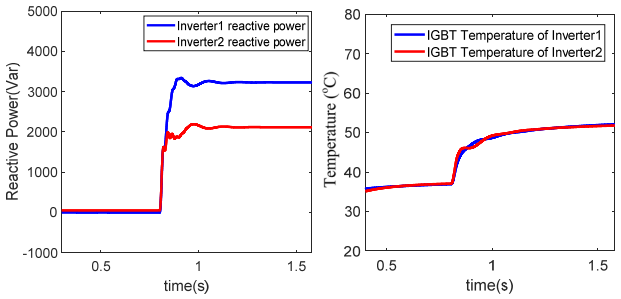

(a) (b)

Fig. 16 Simulated results of paralleled inverters with different power devices. (a) Reactive power sharing of inverters. (b) IGBT average junction temperature of inverters.

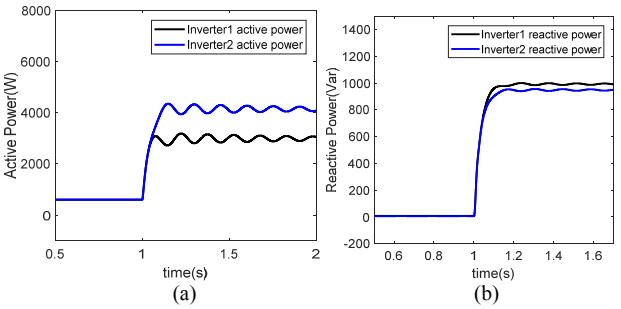

(a) (b)

Fig. 17 Simulation results about output powers of inverter1 and inverter2 in unstable case. (a) Active power sharing of inverters. (b) Reactive power sharing of inverters

V. Experimental Verification

To further validate effectiveness of the proposed droop control strategy, experimental verification is implemented in a scaled-down islanded microgrid with two inverters. The circuit diagram of exemplified microgrid is shown in Fig. 2. The circuit parameters of experimental prototype are same as simulation parameters given in Table II. The scaled down platform in laboratory is shown in Fig.18, which is controlled by dSPACE 1006. Thermal camera is used to identify thermal distribution characteristics of paralleled inverters.

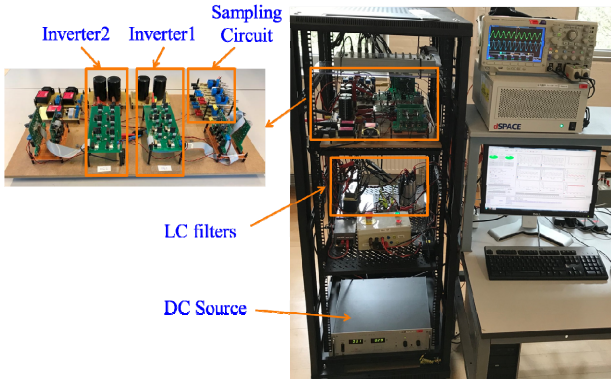

Fig.18. Photo of experimental setup

Fig.19 shows experimental results about output current (Phase A) of paralleled inverters when active power and reactive power loads are increased under conventional droop control strategy, which shows the loads power can be equally shared. Fig. 20 shows experimental results about thermal distribution characteristics of paralleled inverters with active power loads and reactive power loads. It can be seen from thermal imaging measurement that the temperature of inverter1 is up to 86.3°C, while the temperature of inverter2 is 71.9°C, where unequal thermal distribution happens due to difference of electro-thermal parameters.

Fig. 21 shows experimental results about output current of paralleled inverters with active power and reactive power loads under the proposed lifetime-oriented droop control strategy. From Fig. 21, it can be seen that output currents are automatically adjusted to balance thermal distribution of paralleled inverters.

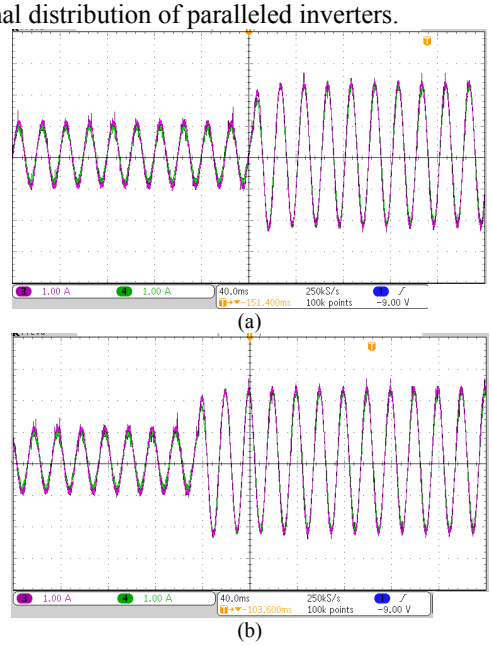

(a)

(b)

Fig. 19. Experimental results about output currents (Phase A) of inverters. (a) Output currents under step disturbance of active power load. (b) Output currents under step disturbance of reactive power load.

This article has been accepted for publication in a future issue of this journal, but has not been fully edited. Content may change prior to final publication. Citation information: DOI 10.1109/TIA.2019.2898847, IEEE Transactions on Industry Applications

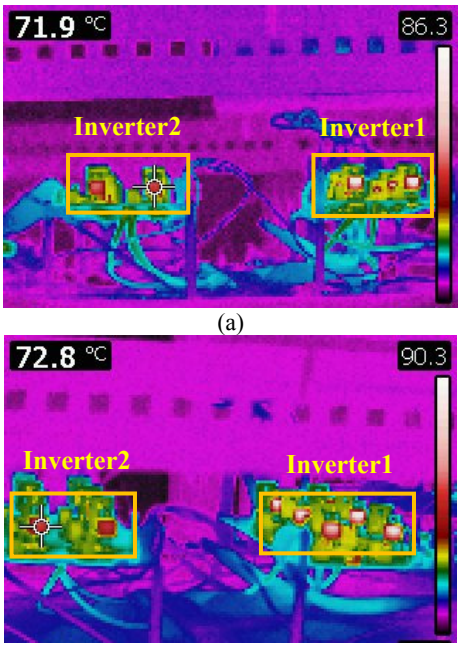

Fig. 20. Thermal distribution characteristics under conventional droop control strategy. (a) Thermal distribution with active power loads. (b) Thermal distribution with reactive power loads.

Fig. 22 shows the experimental results about thermal distribution characteristics of paralleled inverters under the proposed lifetime-oriented droop control strategy. The thermal imaging measurement from Fig. 22 (a) shows that the temperature characteristics of inverter1 and inverter2 are identical, which means that the thermal stress are equally distributed by applying proposed droop control strategy. Also, the Fig. 22(b) shows thermal distribution characteristics of paralleled inverters with reactive power loads under the proposed droop control strategy. The thermal imaging measurement shows that the temperatures of inverter1 and inverter2 are about 71°C. Thermal stress is then equally shared among paralleled inverters.

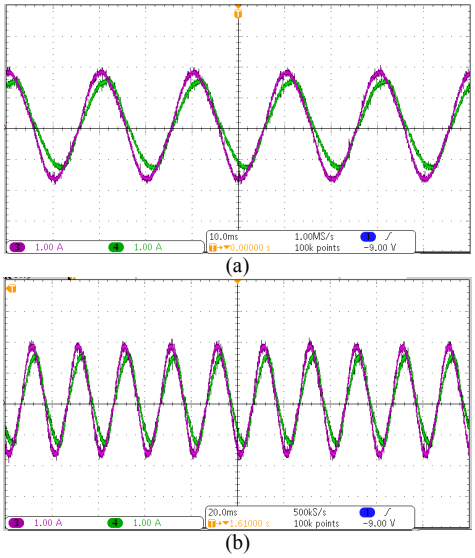

Fig. 21. Experimental results under the proposed oop control strategy. (a) Output currents (Phase A) of paralleled inverters with active power loads. (b) Output currents (Phase A) of paralleled inverters with reactive power loads.

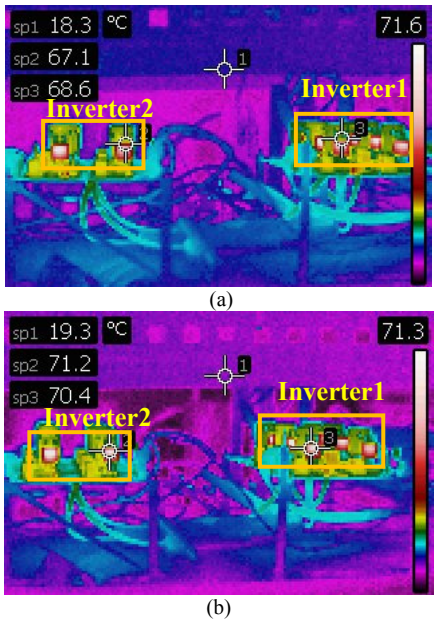

Fig. 22. Thermal distribution characteristics under the proposed lifetime-oriented droop control strategy. (a) Thermal distribution characteristics with active power loads. (b) Thermal distribution characteristics with reactive power loads.

The simulation from Fig.11-16 and experimental verification from Fig. 19-22 show that the proposed droop control is identical with conventional droop control when power devices of different inverters are ideally same. However, once the differences of power devices happen in different inverters, unequal thermal distribution can be caused under conventional droop control. Then, the lifetime-oriented droop control can be activated to implement equal thermal sharing among paralleled inverters. Hence, the proposed lifetime-oriented droop control is an effective complementary for conventional droop control when the differences of power devices occur in practical operation. In the proposed droop controller, only power reference commands are changed according to thermal characteristics of power devices, where the changes of hardware circuit and control loop are not required. Hence, the proposed droop control can be easily implemented.

VI. Conclusion

A lifetime-oriented droop control strategy is developed in this paper. Electro-thermal model is first established to estimate temperature characteristics of different inverters. And temperature-power droop relationship is built according to the electro-thermal model. Then, the lifetime-oriented droop controller is developed to perform identical thermal distribution. In addition, small signal model of microgrid equipped with the proposed droop controller is established, and the effect of electro-thermal parameters of power devices on small signal stability is investigated. Also, closed-loop stability of the proposed droop controller is investigated. Simulation and experimental results verify that the proposed control strategy not only can preserve inherent advantages of conventional droop control strategy but also can achieve identical thermal stress distribution by regulating output powers of inverters. The proposed method thus enhances

This article has been accepted for publication in a future issue of this journal, but has not been fully edited. Content may change prior to final publication. Citation information: DOI 10.1109/TIA.2019.2898847, IEEE Transactions on Industry Applications

the average lifetime and improves long term reliability of microgrids.

APPENDIX

TABLE III
INITIAL CONDITIONS FOR SMALL-SIGNAL STABILITY ANALYSIS

Parameters	Value	Parameters	Value
$[\omega_{10}, \omega_{20}]$	[313.9,313.9]	$[V_{od10}, V_{od20}]$	[150,150]
$[i_{od10}, i_{od20}]$	[6.5,6.5]	$[V_{oq10}, V_{oq20}]$	[0,0]
$[I_{oq10}, I_{oq20}]$	[0.6,0.6]	V_{nom}	150V
$[P_{10}, P_{20}]$	[4000,4000]	$[Q_{10}, Q_{20}]$	[2500,2500]
r_N	1000 Ω		

Parameter matrices of small signal model (37) are given as follows.

$$A_{invi}=\begin{bmatrix}0&k_1&0&0&0&0&0&0&0\\0&k_2&0&k_3&k_4&k_5&k_6&0&0\\0&0&k_7&k_8&k_9&k_{10}&k_{11}&0&0\\0&k_{12}&0&k_{13}&k_{14}&k_{15}&k_{16}&0&0\\0&0&0&0&0&0&0&0&0\\0&0&0&k_{17}&0&k_{18}&k_{19}&k_{20}&0\\0&0&0&0&k_{21}&k_{22}&k_{23}&k_{24}&0\\0&k_{25}&0&k_{26}&k_{27}&k_{28}&k_{29}&0&0\\0&0&k_{30}&k_{31}&k_{32}&k_{33}&k_{34}&0&0\end{bmatrix}$$

$k_1=m_i, k_2=-\omega_c, k_3=\omega_c\cdot i_{odi0}, k_4=\omega_c\cdot i_{oqi0}, k_5=\omega_c\cdot V_{odi0},$

$k_6=\omega_c\cdot V_{oqi0}\quad k_7=-\omega_c\ ,\ k_8=\omega_c\cdot i_{oqi0}\ ,\ k_9=-\omega_c\cdot i_{odi0}\ ,$

$k_{10}=-\omega_c\cdot V_{oqi0}\ ,\ k_{11}=\omega_c\cdot V_{odi0}\ ,\ k_{12}=-\omega_c\cdot n_i\ ,$

$k_{13}=n_i\cdot\omega_c\cdot i_{oqi0}\ ,\ k_{14}=-n_i\cdot\omega_c\cdot i_{odi0}\ ,\ k_{15}=-n_i\cdot\omega_c\cdot V_{oqi0}\ ,$

$k_{16}=n_i\cdot\omega_c\cdot V_{odi0}\quad k_{24}=i_{odi}\cdot\frac{\omega_{\max}-\omega_{\min}}{P_{\max}(T_{IGBT\_\max})}\ ,\ k_{17}=\frac{1}{L_{ci}}\ ,$

$k_{18}=-\frac{R_{ci}}{L_{ci}}\ ,\ k_{19}=-\omega_{i0}\ ,\ k_{20}=i_{oqi}\cdot\frac{\omega_{\max}-\omega_{\min}}{P_{\max}(T_{IGBT\_\max})}\ ,k_{21}=\frac{1}{L_{ci}}\ ,$

$k_{22}=\omega_{i0}\ ,\ k_{23}=-\frac{R_{ci}}{L_{ci}}\ ,\ k_{25}=-\frac{(2a_1P_{i0}+b_1)}{V_{nom}}\omega_c\ ,$

$k_{26}=\frac{(2a_1P_{i0}+b_1)}{V_{nom}}\omega_c\cdot i_{odi0}\ ,\ k_{27}=\frac{(2a_1P_{i0}+b_1)}{V_{nom}}\omega_c\cdot i_{oqi0}\ ,$

$k_{28}=\frac{(2a_1P_{i0}+b_1)}{V_{nom}}\omega_c\cdot V_{odi0}\ ,\ k_{29}=\frac{(2a_1P_{i0}+b_1)}{V_{nom}}\omega_c\cdot V_{oqi0}\ ,$

$k_{30}=-\frac{(2a_1Q_{i0}+b_1)}{V_{nom}}\omega_c\ ,\ k_{31}=\frac{(2a_1Q_{i0}+b_1)}{V_{nom}}\omega_c\cdot i_{oqi0}\ ,$

$k_{32}=-\frac{(2a_1Q_{i0}+b_1)}{V_{nom}}\omega_c\cdot i_{odi0}\ ,\ k_{33}=-\frac{(2a_1Q_{i0}+b_1)}{V_{nom}}\omega_c\cdot V_{oqi0}\ ,$

$k_{34}=\frac{(2a_1Q_{i0}+b_1)}{V_{nom}}\omega_c\cdot V_{odi0}$

$$B_{invi}=\begin{bmatrix}0&0&0&0&0&\frac{1}{L_{ci}}&0&0&0\\0&0&0&0&0&0&\frac{1}{L_{ci}}&0&0\end{bmatrix}^T\quad A_{Load1}=\begin{bmatrix}-i_{LoadQ0}\\i_{LoadD0}\end{bmatrix}$$

$$A_{Load2}=\begin{bmatrix}\frac{-R_{Load}}{L_{Load}}&-\omega_0\\\omega_0&\frac{-R_{Load}}{L_{Load}}\end{bmatrix}\quad A_{Load3}=\begin{bmatrix}\frac{1}{L_{Load}}&0\\0&\frac{1}{L_{Load}}\end{bmatrix}$$

The parameters matrix in (40) is given as following.

$$A_{MG}=\begin{bmatrix}A_1&A_2&A_3\\A_4&A_5&A_6\\A_7&A_8&A_9\end{bmatrix},\ R_N=\begin{bmatrix}r_N&0\\0&r_N\end{bmatrix}$$

$A_1=A_{inv1}+B_{inv1}R_NT_1,\ A_2=B_{inv1}R_NT_2, A_3=B_{inv1}R_N$

$A_4=B_{inv2}R_NT_1,\ A_5=A_{inv2}+B_{inv2}R_NT_2, A_6=B_{inv2}R_N, T_3=m_1x_{inv1}$

$A_7=A_{Load1}T_3+A_{Load3}R_NT_1,\ A_8=A_{Load3}R_NT_2,\ A_9=A_{Load2}+A_{Load3}R_N$

$$T_1=\begin{bmatrix}0&0&0&0&0&1&0&0&0\\0&0&0&0&0&0&1&0&0\end{bmatrix}, T_2=\begin{bmatrix}0&0&0&0&0&1&0&0&0\\0&0&0&0&0&0&1&0&0\end{bmatrix}$$

ACKNOWLEDGEMENT

The authors would like to thank for financial support from ForsKEL and EUDP project ‘‘Voltage control and protection for a grid towards 100% power electronics and cable network (COPE)’’ (No. 880063).

REFERENCES

[1] R. Lasseter, "Smart distribution: Coupled microgrids, " *Proc. IEEE*, vol. 99, no. 6, pp. 1074-1082, Jun. 2011.

[2] Y. Wang, Z. Chen, X. Wang, Y. Tian, Y. Tan, C. Yang, "An estimator-based distributed voltage predictive control strategy for AC islanded microgrids." *IEEE Trans. Power Electron.*, vol. 30, no. 7, pp. 3934-3951, July. 2015.

[3] J. He, Y. W. Li, and F. Blaabjerg, "An enhanced islanding microgrid reactive power, imbalance power, and harmonic power sharing scheme." *IEEE Trans. Power Electron.*, vol. 30, no. 6, pp. 3389-3400, Jun. 2015.

[4] J. Kim, J. M. Guerrero, P. Rodriguez, R. Teodorescu, and K. Nam, “Mode adaptive droop control with virtual output impedances for an inverter-based flexible AC microgrid,” *IEEE Trans. Power Electron.,* vol. 26, no. 3, pp. 689-701, Mar. 2011.

[5] I. U. Nutkani, P. C. Loh, P. Wang, and F. Blaabjerg, "Cost-priorized droop schemes for autonomous AC microgrids." *IEEE Trans. Power Electron.*, vol. 30, no. 2, pp. 1109-1119, Feb. 2015.

[6] Y. Wang, Z. Chen, and F. Deng, “Dynamic droop scheme considering effect of intermittent renewable energy source”. *in Proc. 2016 IEEE 7th International Symposium on Power Electronics for Distributed Generation Systems*, 2016, pp. 1-6.

[7] M. R. Hossain, and H. L. G III, "Real-time distributed coordination of power electronic converters in a DC shipboard distribution system." *IEEE Trans. on Energy Conversion*, vol. 32, no. 2, pp. 770-778, Jun. 2017.

[8] F. Gao, B. Bozhko, and S. Yeoh, G. Asher, and P. Wheeler. "Stability of multi-source droop-controlled electrical power system for more-electric aircraft." *in Proc. 2014 IEEE International Conference on Intelligent Energy and Power Systems*, 2014, pp. 122-126.

[9] D. A. Murdock, J. E. R. Torres, J. J. Connors, and R. D. Lorenz, "Active thermal control of power electronic modules." *IEEE Trans. on Ind. Applications*, vol. 42, no. 2, pp. 552-558, March. 2006.

[10] C. J. J. Joseph, M. R. Zolghadri, A. Homaifa, F. C. Lee, and R. D. Lorenz, “A novel thermal based current sharing control of parallel converters”. *in Proc. 2004 26th Annual International Telecommunications Energy Conference*, 2004, pp. 647-653.

[11] K. Ma, M. Liserre, F. Blaabjerg and T. Kerekes, "Thermal loading and lifetime estimation for power device considering mission profiles in wind power converter." *IEEE Trans. Power Electron.*, vol. 30, no. 2, pp. 590-602, Feb. 2015.

[12] X. Yu, A. M. Khambadkone, H. Wang, and S. T. S. Terence. "Control of parallel connected power converters for low voltage microgrid—Part I: A hybrid control architecture." *IEEE Trans. Power Electron.,* vol. 25, no. 12, pp. 2962-2970, 2010.

[13] H. Wang, A. M. Khambadkone, and X. Yu. "Control of parallel connected power converters for low voltage microgrid—Part II: Dynamic electro-thermal modeling." *IEEE Trans. Power Electron.,* vol. 25, no. 12, pp. 2971-2980, Dec. 2010.

[14] Y. Wang, D. Liu, Z. Chen, F. Deng, and D. Zhou, “Lifetime-oriented droop control strategy for AC islanded microgrids,” in *Proc. ECCE-Asia*, May 20-24, 2018, pp. 1-6.

[15] Infineon Technical Documentation. "Dimensioning program IPOSIM for loss and thermal calculation of infineon IGBT modules."
[16] S. Rohner, S. Bernet, M. Hiller, and R. Sommer, "Modulation, losses, and semiconductor requirements of modular multilevel converters." *IEEE Trans. on Ind. Electron*., vol. 57, no. 8, pp. 2633-2642, Aug. 2010.
[17] N. Baker, M. Liserre, L. Dupont, and Y. Avenas, "Improved reliability of power modules: A review of online junction temperature measurement methods." *IEEE Industrial Electronics Magazine*, vol. 8, no. 3, pp. 17-27, Sep. 2014.
[18] ''IGBT modules technical information'', FS6R06VE3_B2, *Infineon datasheet*, 2007.
[19] ''IGBT modules technical information'', FP10R06KL4, *Infineon datasheet*, 2007.
[20] J. He, Y. W. Li, J. M. Guerrero, F. Blaabjerg, and J. C. Vasquez, "An islanding microgrid power sharing approach using enhanced virtual impedance control scheme." *IEEE Trans. Power Electron.*, vol. 28, no. 11, pp. 5272-5282, Nov. 2013.
[21] N. Pogaku, M. Prodanovic, and T. C. Green, "Modeling, analysis and testing of autonomous operation of an inverter-based microgrid," *IEEE Trans. Power Electron.*, vol. 22, no. 2, pp. 613-625, Mar. 2007.
[22] J. Kim, J. M. Guerrero, P. Rodriguez, R. Teodorescu, and K. Nam, "Mode adaptive droop control with virtual output impedances for an inverter-based flexible AC microgrid," *IEEE Trans. Power Electron.,* vol. 26, no. 3, pp. 689-701, Mar. 2011.
[23] X. Lu, J. M. Guerrero, K. Sun, and J. C. Vasquez, "An improved droop control method for DC microgrids based on low bandwidth communication with DC bus voltage restoration and enhanced current sharing accuracy," *IEEE Trans. Power Electron.,* vol. 29, no. 4, pp. 1800-1812, Apr. 2014.
[24] N. Bottrell, M. Prodanovic, and T. C. Green, ''Dynamic stability of a microgrid with an active load,'' *IEEE Trans. Power Electron.,* vol. 28, no. 11, pp. 5107-5119, Nov. 2013.
[25] Y. Wang, X. Wang, F. Blaabjerg, and Z. Chen, ''Harmonic instability assessment using state-space modeling and participation analysis in inverter-fed power systems,'' *IEEE Trans. Ind. Electron.*, vol. 64, no. 1, pp. 806-816, Jan. 2017.
[26] R. Majumder, B. Chaudhuri, A. Ghosh, R. Majumder, G. Ledwich, and F. Zare, "Improvement of stability and load sharing in an autonomous microgrid using supplementary droop control loop," *IEEE Trans. Power Syst.*, vol. 25, no. 2, pp. 796-808, May. 2010.